*Korean J. Chem. Eng.*, 38(8), 1733-1745 (2021)
DOI: 10.1007/s11814-021-0824-2

pISSN: 0256-1115
eISSN: 1975-7220

# Effects of the content 4,4′-diaminodiphenyl methane on thermomechanical properties of shape-memory epoxy polymers

**Kaixiao Cui, Guancheng Jiang†, Guoshuai Wang, Lili Yang†, and Xiulun Shen**

State Key Laboratory of Petroleum Resources and Prospecting, MOE Key Laboratory of Petroleum Engineering, China University of Petroleum (Beijing), Beijing 102249, China
(*Received 17 January 2021 • Revised 7 April 2021 • Accepted 26 April 2021*)

**Abstract**−A series of thermosetting shape memory epoxy polymers (SMEPs) were prepared using the epoxy resin diglycidyl ether bisphenol A E-51 with varying content of curing agent 4,4′-diaminodiphenyl methane (DDM). The chemical, thermal and mechanical properties of the SMEPs were systematically investigated via Fourier transform infrared spectroscopy, differential scanning calorimetry, dynamic and static mechanical analysis, and thermogravimetric analysis. The results indicate that the shape-memory temperature ($T_g$) of the SMEPs varies within the range of 33.9 °C to 140.0 °C with DDM content increasing from 12% to 25%, and the $T_g$ values exhibit a good linear correlation, with a correlation coefficient of more than 0.999. This indicates that SMEPs with tunable shape-memory temperatures can be realized by controlling the content of the curing agent. When the DDM content is 17-19%, the shape fixity and shape recovery ratio of the SMEPs reaches approximately 100%. In addition, the shape recovery time decreases as temperature increases. This work also highlights the effect of DDM curing agent content on the thermal, mechanical and shape-memory properties of SMEPs, and it is in favor of extending their further applications.

Keywords: Shape-memory Polymer, Shape-memory Effect, Epoxy Resin, Glass Transition Temperature

## INTRODUCTION

Memory-functional polymer materials include those that exhibit stress memory, shape memory, volume memory, and color memory. Among these materials, shape memory polymers (SMPs) have received increasing attention in different applications, particularly in the biomedical, construction engineering and aerospace fields, due to their considerable scientific and technological significance [1-5]. SMPs represent a type of responsive polymer that can change its original shape and maintain a deformed temporary shape and then recover original shape under external stimuli [6]. The characteristic of 'original state, to deformed state, to original state' of these polymers is called the "shape memory effect" [7]. Since the 1980s, several polymers with shape memory behavior have been discovered, including polyurethanes [8,9], polynorbornenes [10], styrene-butadiene copolymers [11], cross-linked polyethylenes [12,13] and shape memory epoxy-based polymers (SMEPs). SMPs can develop a shape memory effect under various external stimuli [5], such as heat, light, magnetism, pH, electricity and moisture. Nevertheless, only SMPs that use heat as stimulus (i.e., thermo-responsive SMPs) have elicited attention due to their easy processing and application. Many temperature-sensitive SMPs with different 'switch' temperatures have been developed. The switch temperature is related to the glass transition temperature ($T_g$) or the melting temperature ($T_m$). Accordingly, SMPs are frequently subdivided into $T_g$-based SMPs with an amorphous phase or $T_m$-based SMPs with a crystalline phase [14-20].

Thermo-responsive SMEPs are among the most attractive SMPs [21-23]. As thermosetting resins, epoxy resins are widely used as coatings, sealants, adhesives in various areas, due to their easy processability, composite moldability, and dimensional stability. Developing methods for conferring shape-memory properties to these versatile resins and extending their applications have attracted the interest of many researchers [22,24]. SMEPs can also be used as matrices that can be reinforced by shape-memory alloys, carbon particles, fibers, nanomaterials, or they can be foamed by gas or hollow glass beads, considerably improving their strength, stiffness and compressibility [25-33]. In addition, SMEPs and their composites are highly attractive for space applications, such as hinges, solar arrays, deployable panels, booms, and reflector-antennas [25,34,35], due to their low outgassing properties, high triggering temperature, high strength-to-weight ratio and good performance when exposed to space radiation.

SMEPs are unique thermosetting SMPs that exhibit excellent shape memory performance (high shape retention and shape recovery rate and fast response) and thermophysical and mechanical properties compared with thermoplastic shape-memory polymers. SMEPs can achieve high shape recovery ratio and excellent mechanical properties. Their thermally reversible segments endow SMEPs with the capability to exhibit shape memory effects [22]. In addition, their shape-memory and mechanical properties can be easily adjusted within a wide range of values to meet different application requirements. Liu et al. [36] studied the preparation of SMEPs based on epoxy resin diglycidyl ether bisphenol A (DGEBA) E-51 with varying content of the curing agent 4,4′-diaminodiphenyl methane (DDM) to determine the $T_g$ of various curing degrees through differential scanning calorimetry (DSC). However, the chemical reac-

†To whom correspondence should be addressed.
E-mail: m15600263100_1@163.com, yangll@cup.edu.cn

tion mechanism between these raw materials and the dynamic and static mechanical properties of a system have not been comprehensively investigated. Song et al. [37] used DDM and m-phenylenediamine as curing agent for epoxy resin E-51 and further found that $T_g$ values vary with characterization methods. SMEPs with good-shape memory performance can also be obtained using other types of curing agents [38]. The aforementioned studies indicate that acquiring good-shape memory capability and mechanical properties for SMEPs depends only on curing agent, that is, the type and content of curing agents will significantly affect the shape memory properties of SMEPs.

To further clarify the effect of curing agent on the SMEPs properties, in this study, in addition to DSC test and shape memory test, we further systematically studied the SMEPs under different curing agent additions via Fourier transform infrared spectroscopy (FT-IR), dynamic mechanical analysis (DMA), static mechanical analysis (SMA), and thermogravimetric analysis (TGA). The chemical composition, dynamic and static mechanical properties in room and high temperature environment, shape memory capacity, and thermal weight loss properties. First, the raw materials and curing procedure used were described in detail. Then, the effects of varying curing agent (DDM) contents on the chemical composition, dynamic and static mechanical properties in room and high temperature environment, shape memory capacity, and thermal weight loss properties of these SMEPs were systematically analyzed. We believe that the results will be highly significant for researchers when using epoxy resin and the curing agent DDM to prepare suitable and reliable shape-memory polymers or composite materials.

## MATERIALS AND METHODS

### 1. Materials

Epoxy resin DGEBA E-51 (Chemical pure) was supplied by Nantong Xingchen Synthetic Material Co., Ltd. Its epoxy equivalent is 186 g/mol, molecular weight is 372 g/mol, epoxy value is 0.5376 mol/100 g, and n value is 0.113. The DDM curing agent (Analytical reagent) was purchased from Sarn Chemical Technology (Shanghai) Co., Ltd. and its molecular weight is 198.264 g/mol.

### 2. Preparation of the SMEPs

The preparation procedure for the SMEPs is illustrated in Fig. 1. After pre-heating to 80 °C, the epoxy resin E-51 was stirred at 200 r/min for 15 min with a magnetic stirrer. Then, a certain amount of DDM curing agent was added and the mixture was stirred for another 10 min at 250 r/min. Thus, a homogeneous solution without any air bubbles was produced. Subsequently, the solution was poured into a polytetrafluoroethylene mold. Beforehand, the mold was placed in a vacuum oven and preheated to 80 °C. The SMEPs were thermally cured at 80 °C for 2.5 h and post-cured at 150 °C for another 2.5 h [37], followed by degassing under a pressure of less than 10 mmHg. Upon the completion of curing, the mold was cooled

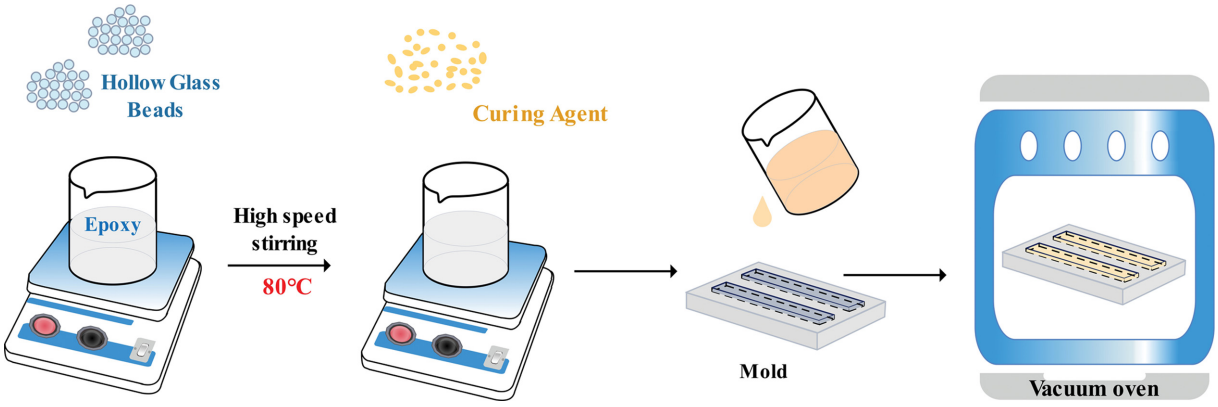


**Fig. 1. Preparation procedure for the SMEPs.**

**Table 1. Formulations of the SMEPs composed of epoxy resin E-51 and DDM curing agent**

| SMEP samples | Epoxy resin E-51 (g) | DDM content (%) | Equivalent ratio of functional groups [epoxy group of E-51] : [amidogen of DDM] |
|---|---|---|---|
| 1 | 100 | 12 | 1 : 0.225 |
| 2 | 100 | 13 | 1: : 0.244 |
| 3 | 100 | 14 | 1 : 0.263 |
| 4 | 100 | 15 | 1 : 0.281 |
| 5 | 100 | 16 | 1 : 0.300 |
| 6 | 100 | 17 | 1 : 0.319 |
| 7 | 100 | 18 | 1 : 0.338 |
| 8 | 100 | 19 | 1 : 0.356 |
| 9 | 100 | 20 | 1 : 0.375 |
| 10 | 100 | 25 | 1 : 0.469 |

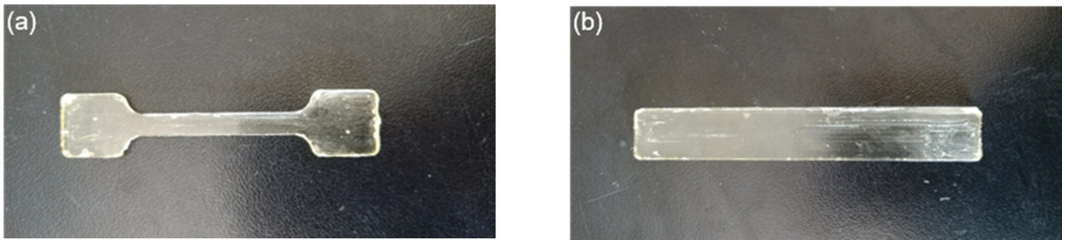


**Fig. 2. Specimens used in mechanical property tests for the SMEPs: (a) Dog-bone specimen for tensile test and (b) rectangular specimen for bending test.**

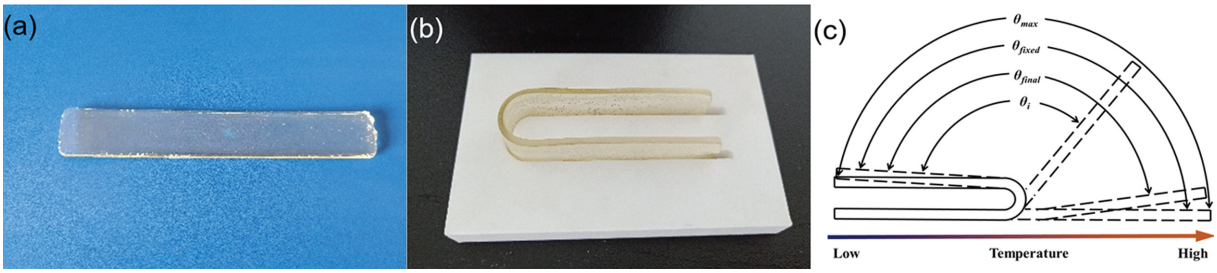


**Fig. 3. Fold-deploy shape memory test of the SMEPs: (a) Original shape state, (b) U-shaped state and (c) illustration of test parameters.**

to ambient temperature and then the SMEPs were removed from the mold. The dimensions of the SMEPs were 150 mm×20 mm×2 mm (length×width×thickness). Nine types of SMEPs with varying DDM contents of 12-20% (by weight of epoxy resin E-51) were prepared. The formulations of SMEPs in this work are summarized in Table 1.

**3. FTIR Test**

The chemical structure of the SMEPs was determined via infrared spectroscopy. The spectra were recorded on a 560 E.S.P FTIR instrument (MAGNA-IR, USA) between 400 $cm^{-1}$ and 4,000 $cm^{-1}$ at a resolution of 4 $cm^{-1}$ via the KBr method under Ar protection.

**4. DMA Test**

Dynamic thermomechanical properties were measured with a Q800 Dynamic Mechanical Thermal Analyzer (TA Instruments, USA), through which the storage modulus (E′), loss modulus (E″), and tangent loss angle (tan$\delta$) were obtained as functions of temperature. A specimen was processed to obtain a size of 35 mm×8 mm×2 mm (length×width×thickness), and then equilibrated at 20 °C and heated to 180 °C at a rate of 4 °C/min. Tests were performed under the three-point bending mode, with a strain amplitude of 60 μm and a frequency of 1 Hz.

**5. SMA Test**

Static mechanical properties were measured on the 5967 Universal Testing System (INSTRON, USA) by tensile and bending tests with a crosshead speed of 2 mm/min. Tensile tests were carried out using dog-bone tensile specimens (the width of the middle area is 5 mm and the thickness is 3 mm) (Fig. 2(a)) at room temperature and high temperature ($T_g$+40 °C), respectively. The bending tests were carried out using rectangular specimens with a size of 100 mm×15 mm×4 mm (length×width×thickness) (Fig. 2(b)) under a three-point bending mode at room temperature.

**6. Fold-deploy Shape Memory Test**

To assess their shape memory capability, the SMEPs were successively subjected to the following evaluation tests [25,36]. First, the SMEPs were heated at 130 °C and then bent into a 'U' shape by encircling a center axis with a diameter of 12 mm in a polytetrafluoroethylene mold, as shown in Fig. 3(a) and Fig. 3(b). The maximum bending angle was recorded as $\theta_{max}$ (here, $\theta_{max}$=180°). Subsequently, the U-shaped SMEPs were cooled to ambient temperature and a constant external force was maintained for several minutes before removal. Marginal recovery occurred, and the as-produced bending angle was termed as $\theta_{fixed}$. Finally, the deformed SMEPs were reheated to recover their original shape. The SMEPs were heated from 25 °C to 120 °C, with a fixed heating rate of 0.5 °C/min and the bending angle "$\theta_i$" was recorded. All related test parameters are illustrated in Fig. 3(c). The shape fixity ($R_f$) and shape recovery ratio ($R_r$) were calculated as follows:

$$R_f = \frac{\theta_{fixed}}{\theta_{max}} \times 100\%, \quad (1)$$

$$R_r = \frac{\theta_i}{\theta_{fixed}} \times 100\%, \quad (2)$$

**7. TGA and DSC Test**

The thermal analysis of the SMEPs was performed on a TGA-DSC1 simultaneous thermal analyzer (METTLER TOLEDO, Switzerland) to examine the thermostability and determine the $T_g$ values. The specimens were heated from 30 °C to 800 °C, at a heating rate of 2 °C/min under $N_2$ protection.

## RESULTS AND DISCUSSION

**1. Chemical Structure of the SMEPs**

Epoxy resin E-51 (Fig. 4(a)) is a viscous liquid and its viscosity decreases with increasing temperature. Without adding any curing agent, such as DDM (Fig. 4(b)), the epoxy resin cannot form a

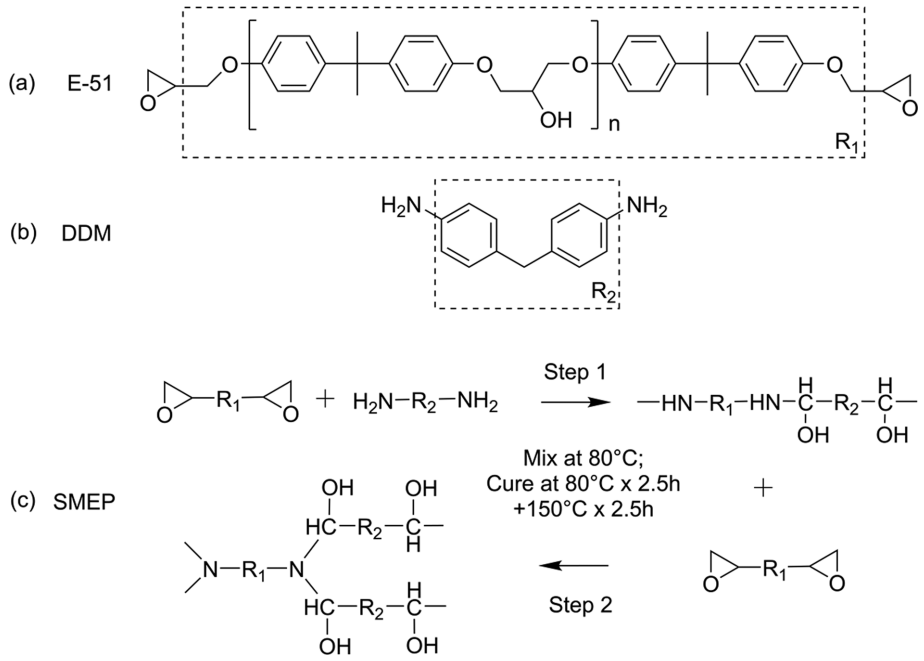


**Fig. 4. Chemical reaction of raw materials: (a) Epoxy resin E-51, (b) DDM and (c) synthesis process of the SMEPs.**

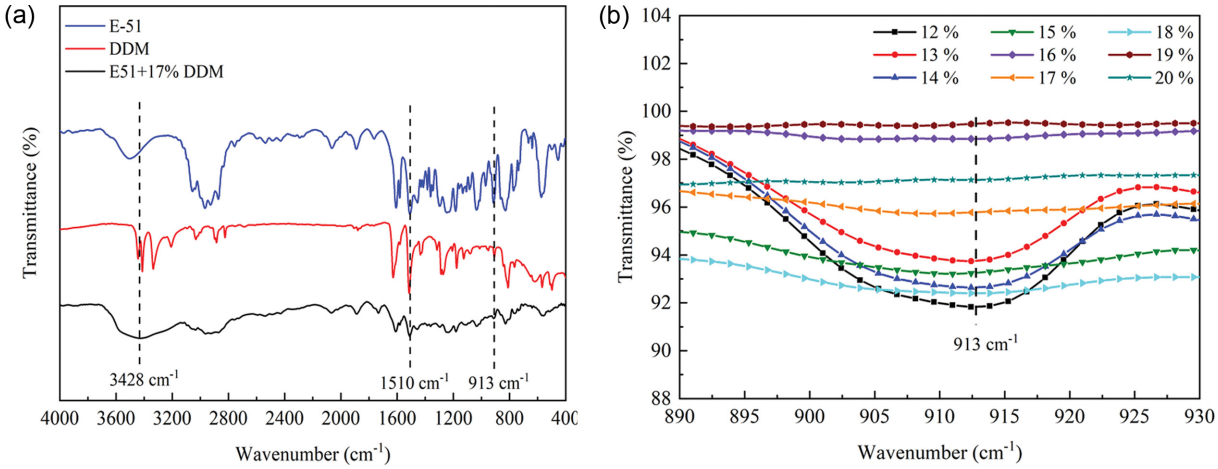


**Fig. 5. Chemical characterization of the SMEPs via FTIR: (a) FTIR curves of E-51, DDM, and the SMEP with 17%DDM content, (b) changing of the characteristic absorption peaks of the epoxy groups at 913 $cm^{-1}$ with DDM contents from 12% to 20%.**

three-dimensional cross-linked network regardless of the setting temperature and time. At high temperature, the active hydrogen in the primary amine groups in DDM reacts with the epoxy groups in E-51, resulting in the formation of a secondary amine group (Step 1). The secondary amine groups further react with the remaining epoxy groups forming tertiary amine groups (Step 2). Ultimately, a three-dimensional cross-linked network is generated (Fig. 4(c)).

The comparison of the infrared spectra of epoxy resin E-51, DDM and the SMEP with 17% DDM content is shown in Fig. 5(a). The stretching vibration peak at 3,428 $cm^{-1}$ is ascribed to the -$NH_2$ or -NH- groups produced in Step 1. Meanwhile, the peak at 1,510 $cm^{-1}$ is attributed to the skeleton vibration peak of a benzene ring or the stretching vibration peak of the C-N bond generated in Step 2. In particular, the intensity of the characteristic peak of the epoxy group near 913 $cm^{-1}$ in E-51 is significantly lower after the reaction, indicating the occurrence of cross-linking process.

To study the effect of DDM content on chemical composition, we compared the infrared spectrum curves around 913 $cm^{-1}$ of SMEPs with DDM content from 12% to 20%. As shown clearly in Fig. 5(b), the characteristic absorption peak of the epoxy groups at 913 $cm^{-1}$ decreases continuously as the amount of DDM increases. This result is attributed to the increased consumption of epoxy groups in E-51 due to the reaction with increasing DDM content.

The curing degree of the SMEPs also continuously increases as DDM content increases. For the curing reaction of epoxy resin E-51 and DDM curing agent, the amount of DDM required for the complete reaction of all epoxy groups ($W_{100}$) is calculated as the following equation:

**Table 2. The curing degree of the SMEPs based on epoxy resin E-51 and DDM curing agent system**

| SMEP samples | 1 | 2 | 3 | 4 | 5 | 6 | 7 | 8 | 9 | 10 |
|---|---|---|---|---|---|---|---|---|---|---|
| DDM content (%) | 12 | 13 | 14 | 15 | 16 | 17 | 18 | 19 | 20 | 25 |
| Curing degree (%) | 45.05 | 48.80 | 52.55 | 56.31 | 60.06 | 63.81 | 67.57 | 71.32 | 75.08 | 93.84 |

$$W_{100}=\frac{M_w E_v}{H_n}, \quad (3)$$

where, $W_{100}$ is the amount of DDM curing agent required for the complete reaction of all epoxy groups, g; $M_w$ is molecular weight of DDM, g/mol, here, the value is 198.264; $E_v$ is the epoxy value of epoxy resin E-51, mol/100 g, here, the value is 0.5376; $H_n$ is the number of reactive hydrogens in DDM, here, the value is 4.

So the amount of DDM curing agent required for the complete reaction of all epoxy groups ($W_{100}$) is 26.65 g. Then, the curing degree ($C_d$) of these SMEP samples can be calculated as the following equation:

$$C_d=\frac{W}{W_{100}}\times 100\%, \quad (4)$$

where, $C_d$ is curing degree of the SMEP samples, %; W is actual amount of curing agent DDM, g.

Table 2 lists the calculated curing degree of the SMEPs. When the DDM content ranged from 12% to 25%, the theoretical curing degree of the SMEPs increased from 45.05% to 93.84%. This condition corresponds to the generation of more cross-linking structures (e.g., covalent bonds) in the SMEPs, and less amount and shorter length of free chain segments.

**2. Glass Transition Temperatures ($T_g$) of the SMEPs**

The DSC measurement of $T_g$ is achieved by testing the change in specific heat capacity. It will produce an overall increase while the polymer undergoes a glass transition process. Glass transition is not a phase transition, so no evident endothermic and exothermic reactions occur. Glass transition appears as a jump or shift of the baseline on the curve. The $T_g$ values obtained from the DSC analysis are summarized in Fig. 6. These results indicate that all

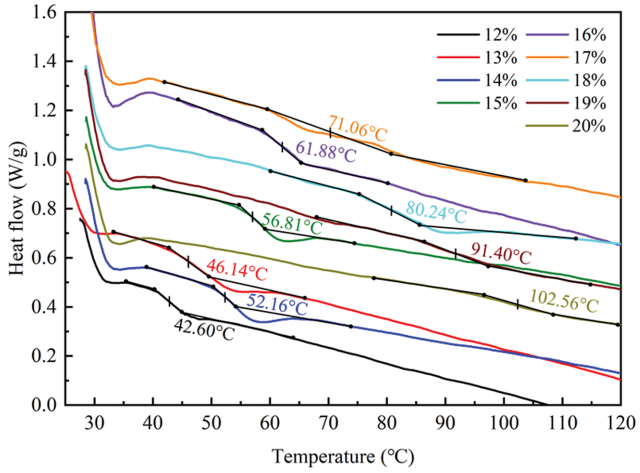


**Fig. 6. DSC curves of the SMEPs with DDM contents varying from 12% to 20%.**

the SMEPs possess distinctive $T_g$ values from 42.60 °C, 46.14 °C, 52.16 °C, 56.81 °C, 61.88 °C, 71.06 °C, 80.24 °C, 91.40 °C to 102.56 °C with DDM content from 12% to 20%. A higher amount of DDM curing agent results in higher cross-linking density and a closer structure, which can hinder the movement of segments during glass transition and thus increase the $T_g$ values.

**3. Thermomechanical Properties of the SMEPs (E′, E″ and tan$\delta$)**

The movement of polymer chains and segments is well known to be temperature-dependent, leading to the temperature-induced mechanical property of polymer materials. When the temperature is considerably lower than $T_g$, large-scale conformational changes are impossible for polymers and only local conformational changes are allowed, similar to when the molecular chains are 'frozen'. Consequently, the stiffness of the polymer is high and the storage modulus is large. For a polymer in glass state, the typical modulus varies between 1 GPa and 10 GPa; when the temperature is above $T_g$, the polymer is in rubbery state, which is in favor of the occurrence of considerable conformation changes. Thus, the polymer becomes soft and its storage modulus is reduced to 1-10 MPa.

The storage modulus E′ curves versus temperature for the SMEPs with different DDM content are shown in Fig. 7(a). At ambient temperature (25 °C), all the SMEPs exhibit similar storage modulus E′ of 2-3 GPa with high stiffness, indicating that they exist in glass state. When temperature exceeds $T_g$, the storage modulus E′ begins to decrease. As temperature further increases, the storage modulus E′ continues to decrease until a certain temperature is reached. From this temperature, the storage modulus E′ remains at a certain value and will not change. At this moment, the SMEPs are soft and exhibit a highly elastic rubbery state. The storage modulus E′ of the SMEPs at high temperatures also differs distinctively from one another depending on the DDM content. At high temperature (above 90 °C), the storage modulus E′ of the SMEP with 12% DDM content is only approximately 0.26 MPa, i.e., it decreases by four orders of magnitude compared with that at ambient temperature. With an increase in DDM content, the storage modulus E′ gradually increases at high temperature. For example, when DDM content is 20% and 25%, the storage modulus E′ reaches 8.45 MPa and 23.31 MPa, corresponding to an increase of three orders and two orders of magnitude compared with that at ambient temperature, respectively. In general, a good SMP should exhibit a change in the storage modulus E′ of more than two orders above and below $T_g$, and an appropriate storage modulus E′ must be achieved to guarantee the required deformation [36]. At high temperature, an excessively high modulus is not conducive to secondary deformation. However, an extremely low modulus may also cause the material to become too soft and thus limit its use. Therefore, the SMEPs with DDM content of 14-19% with three orders of change in the storage modulus are considered ideal SMP materials.

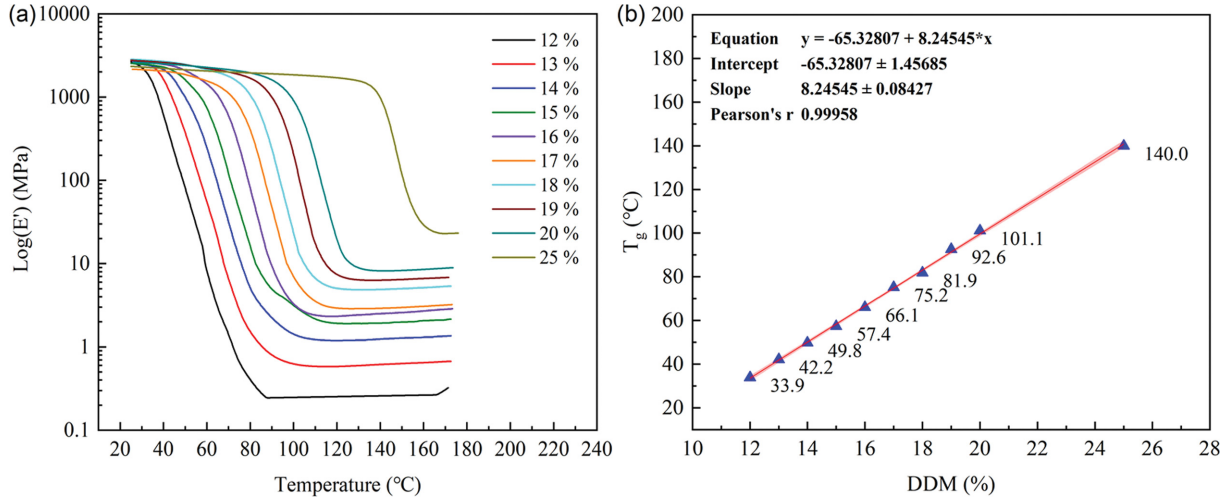


**Fig. 7. (a) Storage modulus E′ of the SMEPs with DDM curing agent content varying from 12% to 25%, and (b) fitting information of $T_g$ determined from the onset temperature of the storage modulus E′ curves.**

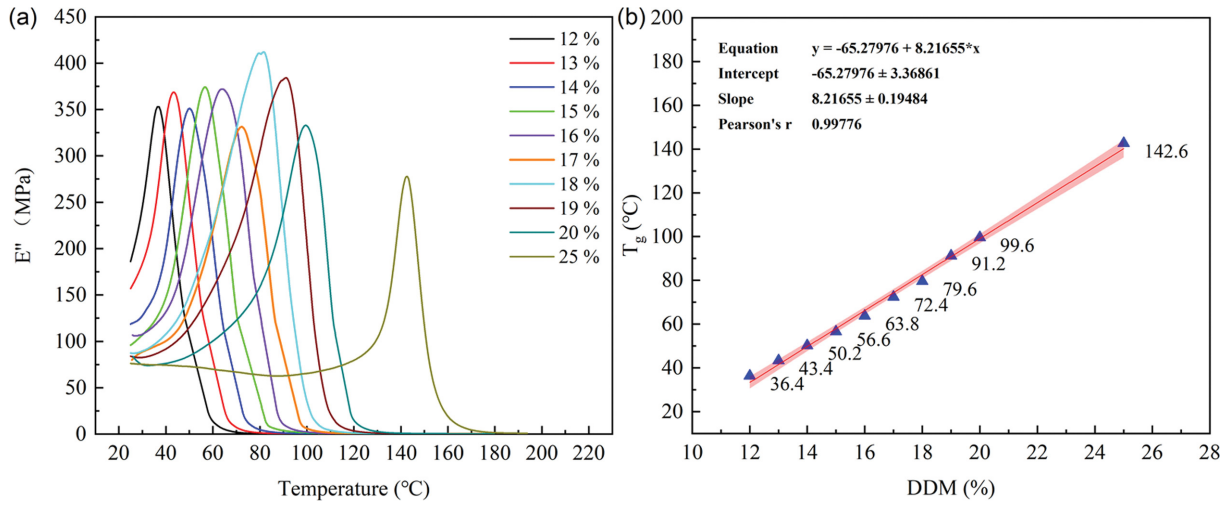


**Fig. 8. (a) Loss modulus E″ of the SMEPs with DDM curing agent content varying from 12% to 25%, and (b) Fitting information of $T_g$ determined from the peak of loss modulus E″ curves.**

The loss modulus E″ curves, as a function of temperature for SMEPs with different DDM content, are presented in Fig. 8(a). During the heating process from glassy state to rubbery state, the loss modulus E″ of all the SMEPs initially exhibits a dramatic increase. Then, they decrease rapidly after reaching the peak values. From the perspective of mechanics, when chain segments are 'frozen' at low temperatures due to few relative migrations between them, overcoming friction between chain segments is no longer necessary. Therefore, the loss modulus E″ value is small. When chain segments move freely at high temperature, the interaction between chain segments is small, and the loss modulus E″ is also not too high. However, to change a chain segment from frozen to free, high friction due to limited space must be overcome. So the loss modulus E″ is high. In particular, the loss modulus E″ reaches its greatest value at $T_g$.

The effect of temperature can also be observed from the tangent loss factor (tan$\delta$) curves (Fig. 9(a)). The tangent loss factor tan$\delta$ of the SMEPs increases in the beginning and then decreases as DDM content increases. The chain segments are subject to internal friction during movement. When the external force changes, the movement of chain segments lags behind the change in external force. Consequently, the deformation lags behind the stress. Then, a phase difference appears. The larger the phase difference, the more difficult the segment movement, and the more it cannot keep up with the change in external force. Thus, the peak height of the tan$\delta$ curve is associated with molecular mobility [36]. Overall, the peak values of the tan$\delta$ curves decrease with increasing DDM content, indicating that molecular mobility decreases.

This phenomenon is largely due to an increase of cross-linking density. The equivalent of effective network chains contained in a unit volume of thermoset elastomer, i.e., the cross-linking density (mol/cm$^3$), is an important characteristic parameter of the cross-linked polymer. According to the cross-linking network theory, with the increase of the crosslinking density, the connections between

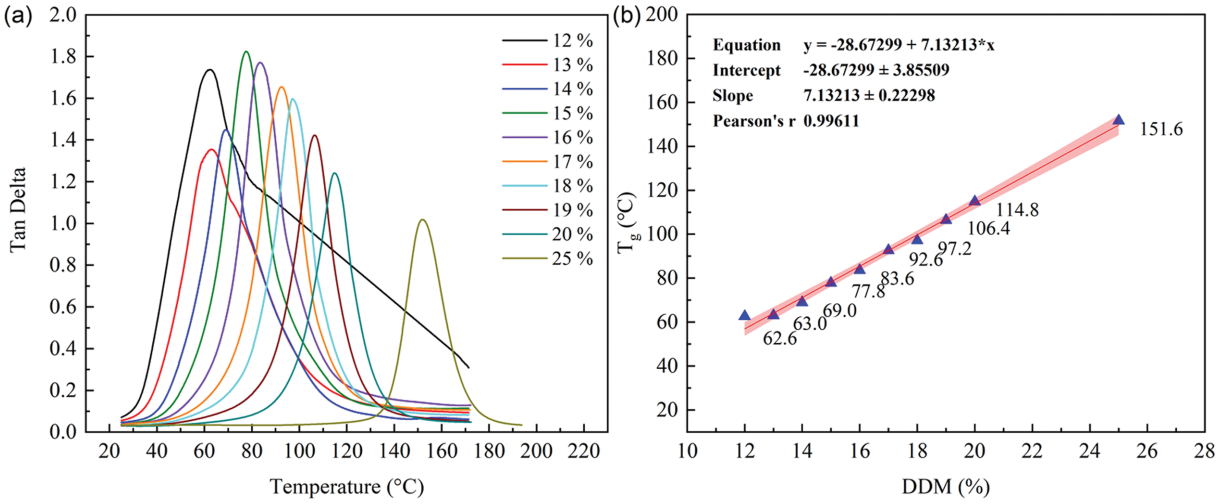


**Fig. 9. (a) Tangent loss factor tan$\delta$ of the SMEPs with DDM content varying from 12% to 25% and (b) fitting information of $T_g$ determined from the peak of the tan$\delta$ curve.**

**Table 3. The cross-linking densities of the SMEPs**

| SMEP samples | DDM content (%) | E at platform area (MPa) | T at $T_g$+40 °C (K) | Cross-linking density $v_e$ ($\times10^{-3}$ mol/cm$^3$) |
|---|---|---|---|---|
| 1 | 12 | 0.256 | 216.68 | 0.237 |
| 2 | 13 | 0.607 | 217.4 | 0.559 |
| 3 | 14 | 1.235 | 228.2 | 0.109 |
| 4 | 15 | 1.952 | 244.04 | 1.604 |
| 5 | 16 | 2.523 | 254.48 | 1.988 |
| 6 | 17 | 2.960 | 270.68 | 2.192 |
| 7 | 18 | 4.997 | 278.96 | 3.591 |
| 8 | 19 | 6.511 | 295.52 | 4.417 |
| 9 | 20 | 8.454 | 310.64 | 5.455 |
| 10 | 25 | 23.312 | 376.88 | 12.400 |

the rubbery molecular chains become a more compact three-dimensional network structure, which limits the movement of the molecular chains. Therefore, under a certain stress, the deformation is small and the modulus is improved. According to the derivation equation of rubber elasticity theory [39,40], the relationship between the crosslinking density $v_e$ and the storage modulus E′ in the platform area at rubbery state is as follows:

$$v_e = \frac{E}{6RT}, \quad (5)$$

where, the $v_e$ is the crosslinking density, mol/m$^3$; E is the storage modulus of the rubber platform area above $T_g$+40 °C, 0.1 Pa; R is the gas constant, 8.314 J/(mol·K); T is the absolute temperature, K.

The cross-linking densities of the SMEPs according to Eq. (5) are listed in Table 3. It can be seen that the cross-linking densities gradually increase with the increasing of DDM curing agent content. When the DDM content is 12%, the cross-linking density is $0.237\times10^{-3}$ mol/cm$^3$. When the DDM content is 20% and 25%, the cross-linking density is $5.455\times10^{-3}$ mol/cm$^3$ and $12.400\times10^{-3}$ mol/cm$^3$. The increase of crosslinking density indicates that the number of cross-linking points in the system increases, and the molecular segments between the cross-linking points become short. This reduces the ability of molecular chain segments to move.

The glass transition temperature $T_g$ values can also be determined from the DMA results, and the effect of DDM curing agent can also be compared. Here, we define the onset temperature as $T_g$ at which the storage modulus curve begins to decrease. The $T_g$ values of the SMEPs obtained from storage modulus curves with DDM curing agent content varying from 12% to 25% are 33.9 °C, 42.2 °C, 49.8 °C, 57.4 °C, 66.1 °C, 75.2 °C, 81.9 °C, 92.6 °C, 101.1 °C and 140.0 °C. The fitting correlation of these $T_g$ values is further analyzed in Fig. 7(b). The fitting equation is '$T_g$ value'=65.32807+8.24545×'DDM content value', and the Pearson's correlation coefficient (R) reaches 0.999. The red area on the linear fitting line shows the 95% confidence interval of the fitting result. The analysis result indicates that the $T_g$ values determined by the storage modulus curves of the SMEPs exhibit excellent linear correlation. The $T_g$ values of the SEMPs can also be determined by the peak values of the loss modulus curves and the tangent loss factor curves. The $T_g$ values determined by loss modulus curves are 36.4 °C, 43.3 °C, 50.2 °C, 56.6 °C, 63.8 °C, 72.4 °C, 79.6 °C, 91.2 °C, 99.6 °C, and 142.6 °C.

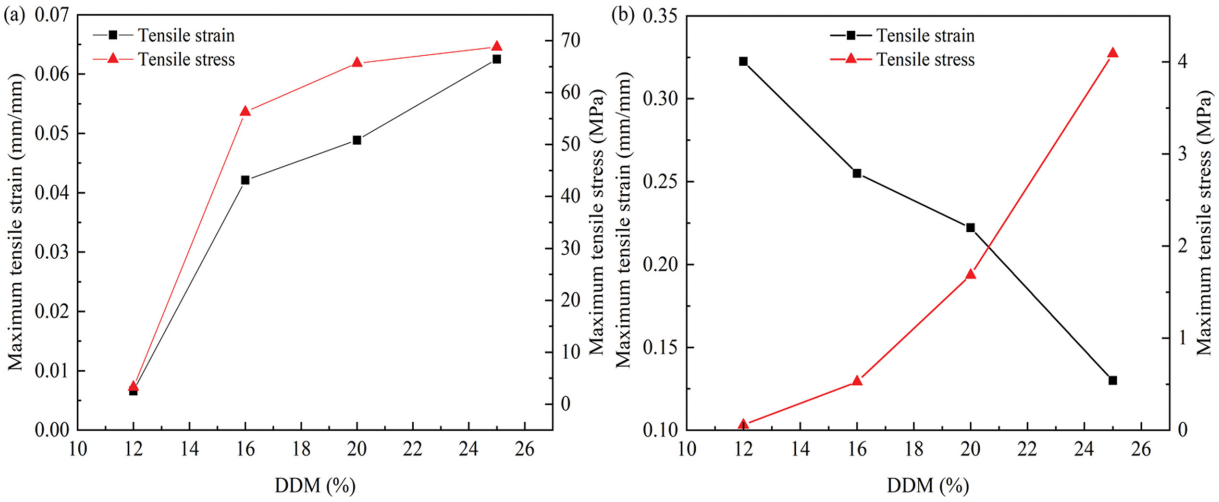


**Fig. 10. Maximum tensile stress and tensile strain of the SMEPs under room temperature (a) and high temperature (b).**

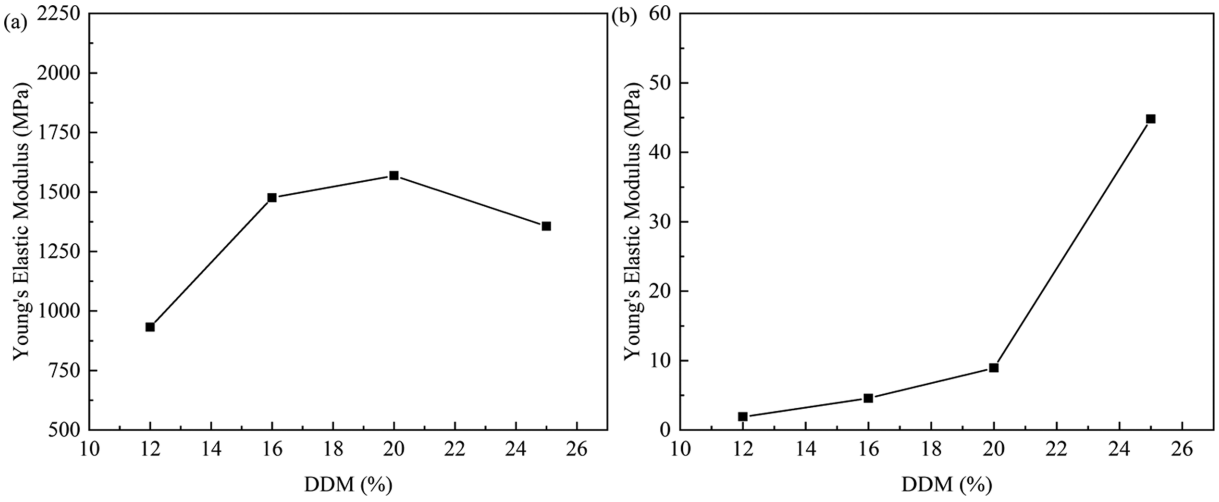


**Fig. 11. Young's elastic moduli of the SMEPs with DDM content varying from 12% to 25% under room temperature (a) and high temperature (b).**

The $T_g$ values determined by the tangent loss factor curves are 62.6 °C, 63.0 °C, 69.0 °C, 77.8 °C, 83.6 °C, 92.6 °C, 97.2 °C, 106.4 °C, 114.8 °C, and 151.6 °C. Furthermore, the fitting curves and equations are also presented in Fig. 8(b) and Fig. 9(b), respectively, and they also exhibit good linear correlation.

## 4. Static Mechanical Properties of the SMEPs

Fig. 10 shows the maximum tensile strength and tensile strain of the SMEPs with different DDM curing agent content at room temperature and high temperature ($T_g$+40 °C (Table 3)). At room temperature, as the amount of DDM increases, the maximum tensile strength of the SMEPs and the maximum tensile strain both gradually increase. When the amount of curing agent increases from 12% to 20%, the tensile strength and tensile strain of the SMEPs increase from 3.31 MPa, 0.007 mm/mm to 65.69 MPa, 0.049 mm/mm, respectively. When DDM content is 25%, the tensile strength and tensile strain are only slightly increased, which are 68.78 MPa and 0.063 mm/mm, respectively. At the same time, Young's elastic modulus of elasticity increased from 931.96 MPa to 1,568.83 MPa. It is worth noting that the modulus of elasticity decreases slightly when 25% DDM is added, and it is 1,355.94 MPa (Fig. 11(a)). Elastic modulus can be regarded as an index to measure the degree of difficulty for a material to produce elastic deformation. The greater its value is, the greater the stress that causes a certain elastic deformation of the material will be, i.e., the greater the material stiffness is. Excessive DDM content (25%) will lead to an increase in the cross-linking density of the system, thus increasing the stiffness and resulting in a decrease in the elastic modulus. When the DDM curing agent content is low (12%), the strength of the SMEPs is due to the low crosslinking density. Only the appropriate content of curing agent (16-20%) can achieve a high modulus of elasticity.

At high temperatures, i.e., at rubbery state, the tensile strength of SMEPs increases with the amount of DDM curing agent, but unlike room temperature the tensile strain gradually decreases. When the amount of DDM curing agent increases from 12% to 25%, the tensile strength increases from 0.06 MPa to 4.09 MPa; however, the tensile strain decreases from 0.322 mm/mm to 0.130 mm/mm

(Fig. 10(b)). This may be because the increase of DDM curing agent content improves the density of the SMEPs, thus improving the strength and reducing the elongation at break. Young's elastic modulus of elasticity also increased significantly with the addition of DDM curing agent from 1.91 MPa to 44.78 MPa. In addition, the tensile strength and elastic modulus at high temperature are lower than that at room temperature, but the tensile strain is higher than that at room temperature. This indicates that the strength of the SMEPs will decrease at high temperature; however, the ductility will increase.

In addition to the tensile properties, the bending properties at room temperature were also investigated (Fig. 12). It can be seen from the results that as the DDM curing agent increases from 12% to 20%, the displacement and load of the SMEPs significantly increase from 1.02 mm, 91.95 N to 8.04 mm and 478.12 N, respectively. The elastic modulus increases from 2,197.06 MPa to 3,250.06 MPa. When the DDM curing agent content further increases to 25%, the displacement and load drop to 6.93 mm, 323.94 N, respectively, and the elastic modulus drops to 2,029.32 MPa. This indicates that the optimal bending strength is obtained when the DDM curing agent content ranges from 16-20%.

**5. Shape Frozen/Recovery Responses of the SMEPs**

The shape memory properties of SMPs are generally determined through cyclic thermomechanical tests that are performed under stress- or strain-controlled conditions. The deformation modes typically cover tension, compression, bending and torsion. In this section, a typical fold-deploy bending test [41] was performed to evaluate the shape memory properties of SMEPs; in this test, the shape fixity $R_f$ and shape recovery ratio $R_r$ are calculated and compared. Here, the shape fixity $R_f$ denotes the fixing extent of the externally applied deformation in the temporary shape. Its value is 100% when the applied deformation introduced above $T_g$ is kept in the temporary shape below $T_g$. The shape recovery ratio $R_r$ indicates the percentage of the recovery of the original shape when an SMEP is subsequently heated in stress-free state (i.e., unconstrained) above $T_g$. The shape recovery ratio $R_r$ is 100% when the

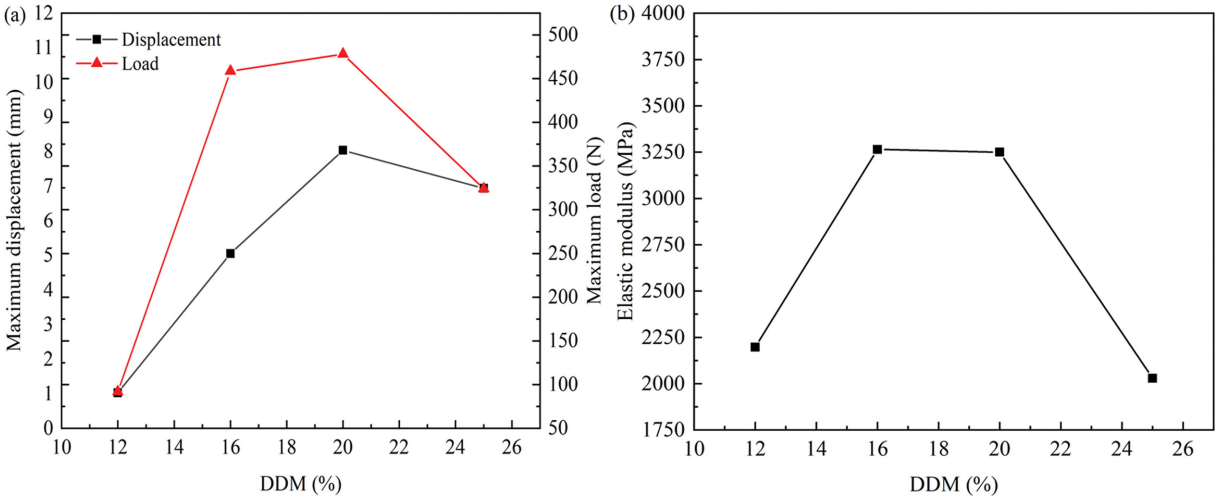


**Fig. 12. Elastic modulus (a) and maximum displacement and load (b) of the SMEPs under room temperature.**

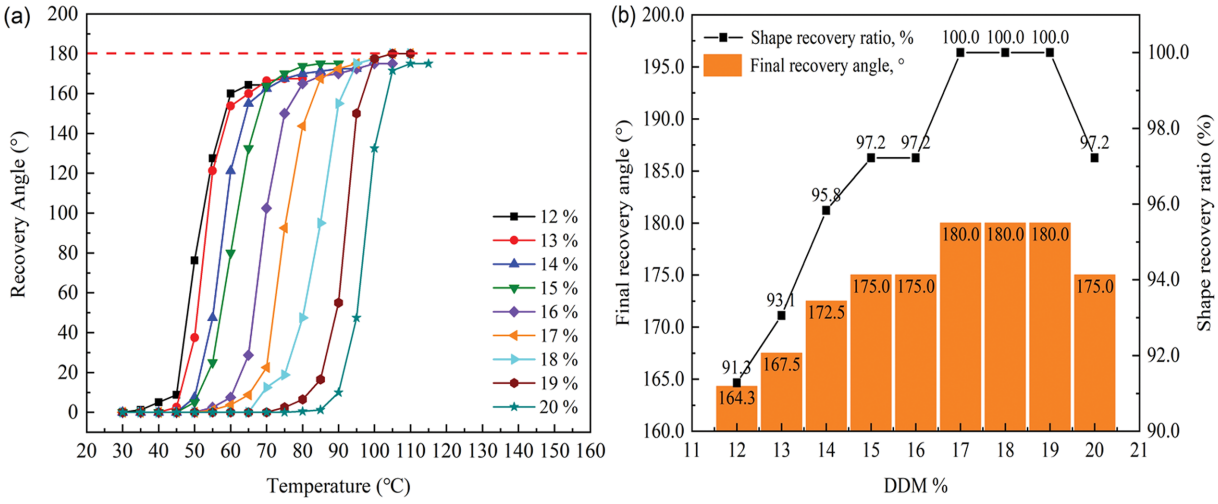


**Fig. 13. Fold-depoly shape memory tests for the SMEPs with DDM varying content from 12% to 20%: (a) Shape recovery angle vs. temperature and (b) final recovery angle and shape recovery ratio vs. DDM content.**

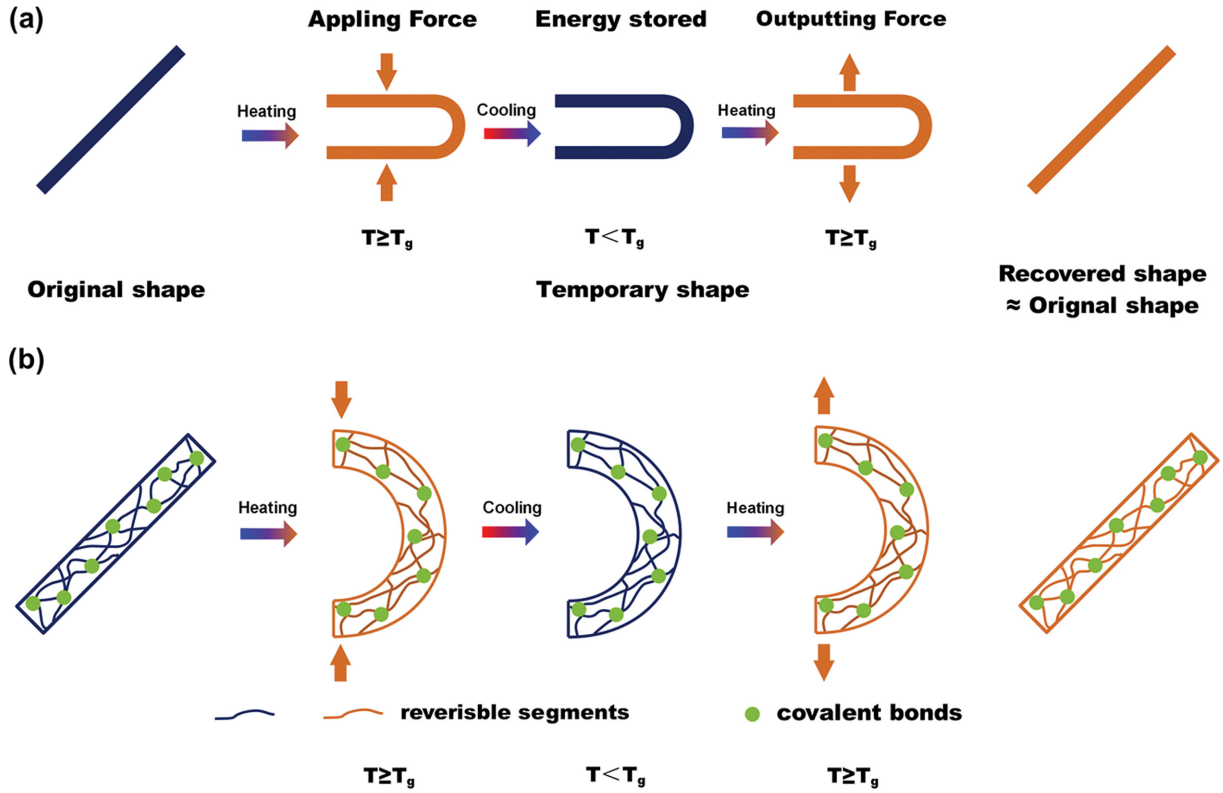


**Fig. 14. Mechanism of the SMEPs' shape-memory effect during the fold-deploy thermomechanical cycle: (a) Schematic of the shape change of the SMEPs and (b) molecular model of the SMEPs.**

original shape, i.e., the implemented energy, is fully restored.

5-1. Shape Fixity

In the test process, only a slight difference existed between $\theta_{fixed}$ and $\theta_{max}$ (more accurately, less than 1°), and thus, all the shape fixity $R_f$ values of the SMEPs were approaching 100%. The excellent shape-fixing capability of epoxy-based SMPs has also been demonstrated by other researchers [36]; such capability is beneficial for the secondary shaping of the SMEPs, i.e. ,memorizing their temporary shape.

5-2. Shape Recovery Ratio

The recovery angle versus temperature curves of the SMEPs are presented in Fig. 13(a). The recovery angles of all the SMEPs exhibit a similar trend. As temperature increases, the recovery angle begins to increase gradually. When temperature continues to increase, the recovery angle rises sharply, gradually reaches the maximum recovery angle and then stops changing with temperature. Although the shape fixity $R_f$ is nearly 100%, the shape recovery ratio $R_r$ exhibits a difference. The final recovery angle and shape recovery ratio $R_r$ of the SMEPs are presented in Fig. 13(b). The shape recovery ratio $R_r$ is strongly related to the DDM curing agent content. In particular, when DDM content is 12%, the shape recovery ratio of this SMEP is 91.3%. When DDM content is 15-16%, the shape recovery ratio reaches as high as 97%. When DDM content is 17-19%, the shape recovery ratio reaches 100%. However, the shape recovery ratio exhibits a downward trend when DDM curing agent content reaches 20%. Therefore, an excessively high or low DDM content may weaken the shape memory effect. This indicates that appropriate cross-linking density is an important factor for shape memory performance and it can be adjusted through DDM content.

For the thermosetting SMEPs, the shape recovery temperature, i.e., transition temperature, is $T_g$. As illustrated in Fig. 14, during the folding process, when the temperature is above $T_g$, the reversible segments between covalent bonds (i.e., crosslinked points) in the SMEPs can adapt to the externally applied force via conformational rearrangements. When the applied force is maintained and the temperature is cooled below $T_g$, the reversible segments are 'frozen' and thus, the strain energy can be stored. When the SMEPs are unloaded and heated above $T_g$ again, the strain energy is released and the permanent shape is restored as a result of the unfreezing of the reversible segments. Therefore, the shape memory effect of the SMEPs is entropic. Nano-indentation test has also demonstrated that the shape memory can persist in extremely small, nanometer-scale volumes in cross-linked epoxy-based polymer networks [42].

5-3. Shape Recovery Temperature

If the shape recovery temperatures are determined as the temperature at which the recovery angle is 90°, i.e., $R_r$ is 50% [37], then the $T_g$ values of the SMEPs with DDM varying content from 12% to 20% are 51.6 °C, 53.0 °C, 58.0 °C, 61.0 °C, 68.0 °C, 75.0 °C, 84.5 °C, 91.5 °C and 97.5 °C. A positively correlated relationship is also observed in the shape recovery temperature of the SMEPs and DDM content. From the microstructure perspective, this result may be attributed to higher cross-linking density due to an increase in DDM content. Therefore, tailored SMEPs with certain shape recovery temperatures are possible to achieve by precisely adjusting

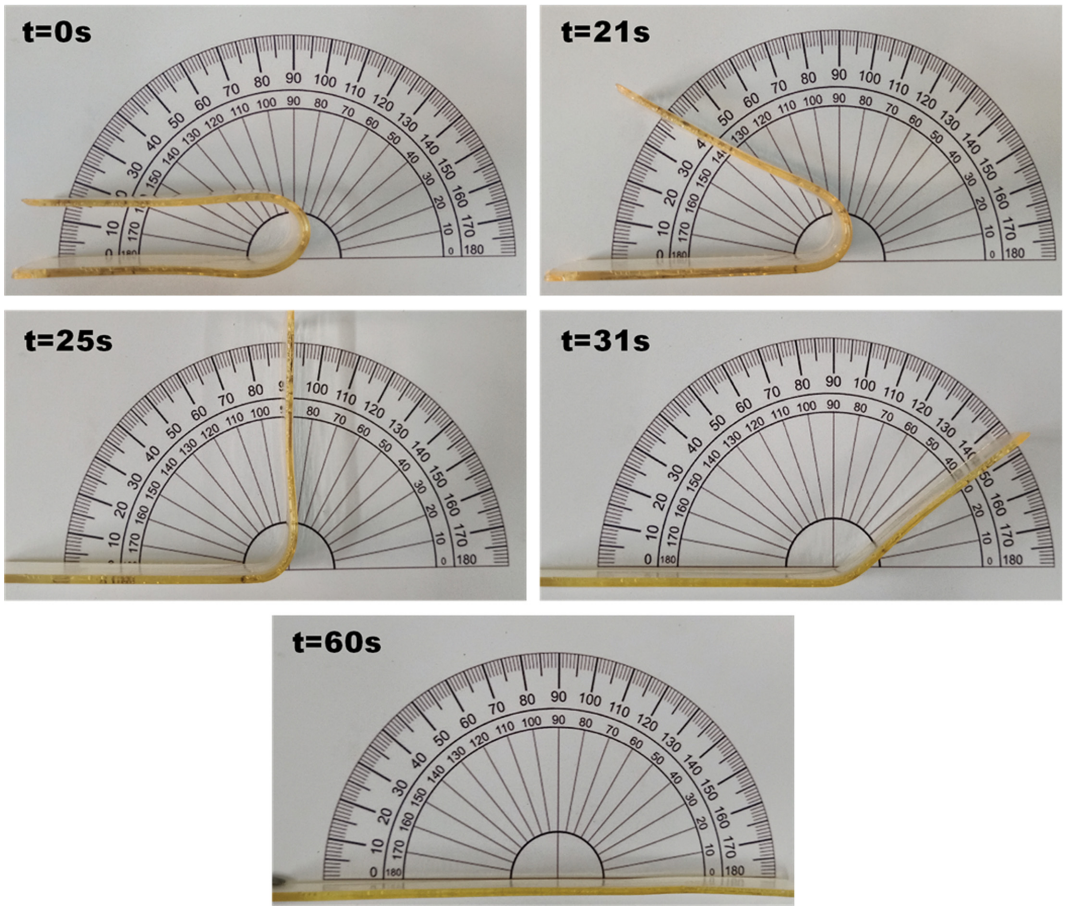


**Fig. 15. Photographs of the shape recovery process of the SMEP with a DDM content of 17% at 95 °C.**

DDM curing agent content.

5-4. Shape Recovery Time

The shape recovery time of SMPs also considerably influences their practical applications. The shape recovery process of the SMEP with 17% DDM curing agent content at 95 °C is illustrated in Fig. 15. At 95 °C, this U-shaped SMEP requires 25 s to return to half (90°), and 60 s to return to its original shape (180°). At increased temperatures, such as 115 °C, time is shortened to 18 s and 29 s, respectively. For the SMEP with 13% DDM content at 73 °C and 93 °C, the recovery time required to return to its original shape (180°) is 80 s and 15 s, respectively. This result indicates that the shape recovery time of the SMEPs decreases as temperature increases. The primary reason is that a higher temperature will promote higher energy gained of the reversible segments inside the SMEPs and better accelerate the segments' thermal motion and shape recovery speed, and thus, less time is required for shape recovery process.

## 6. Comparison of $T_g$ Values Obtained by Different Methods

The shape recovery temperature of SMPs is an important parameter for application. For thermosetting SMEPs, the shape memory temperature is essentially the glass transition temperature $T_g$. In terms of molecular structure, the glass transition is a relaxation phenomenon from the 'frozen' state to the 'defrosted' state of the amorphous part of the polymer. There is no phase change heat like the phase transition, so it is a kind of secondary phase transition (main transition). Below $T_g$, the SMEP is in a glassy state and the molecular chain segments barely cannot move, but the atoms (or groups) vibrate at their equilibrium positions. Above $T_g$, the chain

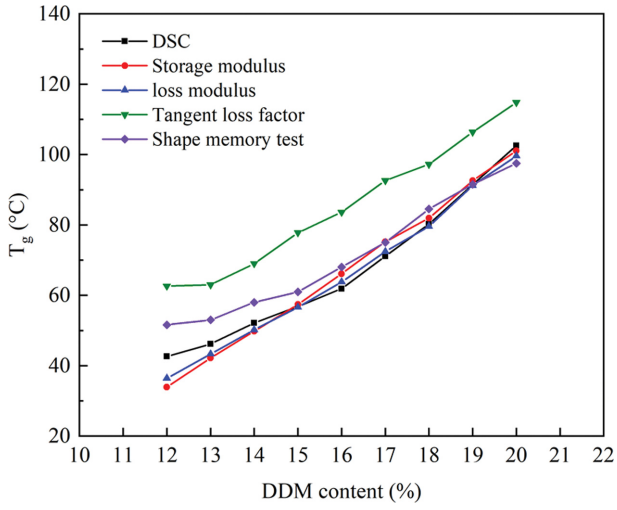


**Fig. 16. Comparison of glass transition temperature $T_g$ obtained from different test methods.**

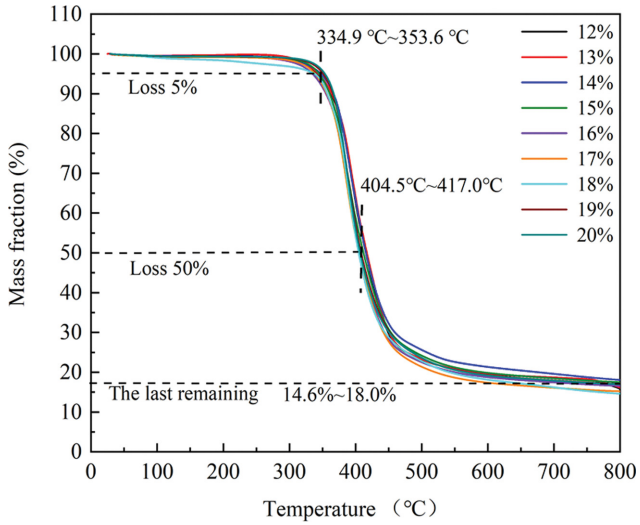


**Fig. 17. Thermal weight loss curves of the SMEPs with DDM curing agent contents.**

segments start to move and exhibit high elasticity. Within $T_g$ range, the specific heat capacity and modulus of the SMEP will change significantly, so it can be analyzed by DSC test and DMA test. Fig. 16 presents a comparison of $T_g$ values of the SMEPs with varying DDM content determined by DSC, DMA (storage modulus, loss modulus, tangent loss factor) and fold-deploy shape memory test. It can be found that $T_g$ values from these methods are different, especially when DDM curing agent content is less than 15%. More specifically, the glass transition temperature $T_g$ from tangent loss factor is 14.61-21.48 °C higher than the others. $T_g$ from storage modulus, loss modulus and DSC is the lowest and the values are roughly the same. $T_g$ from shape memory test is at the medium location. We found that the $T_g$ from DSC is about 18 °C lower than that from DMA (tangent loss factor) and the difference may mainly due to the frequency effect in DMA test and phase difference [36]. The fold-deploy shape memory test is a time-consuming process, which may cause some delay. The storage modulus and loss modulus sensitively reflect the elastic properties of SMEPs under dynamic and heated conditions, which cause the $T_g$ values to have the lowest value.

**7. Thermosability of the SMEPs**

The thermal weight loss curves of the SMEPs are presented in Fig. 17. No significant difference exists in various SMEPs with different DDM content. In general, the decomposition temperature of the 5% weight loss of the SMEPs is 334.894-353.595 °C. The decomposition temperature of the 50% weight loss is 404.532-417.057 °C. The residual carbon mass fraction of the SMEPs at 600-800 °C is 14.606-18.063%. These results can provide references for selecting the application temperatures of the SMEPs.

## CONCLUSIONS

A series of SMEPs were synthesized with tunable shape memory temperatures by controlling the DDM curing agent content in epoxy resin E-51. The amine groups in DDM react with the epoxy groups in epoxy resin E-51, generating a three-dimensional network structure. As DDM content increases, the curing degree and cross-linking densities of the SMEPs continuously increase, significantly affecting the dynamic and static mechanical and shape memory properties of the SMEPs, particularly the shape-memory temperature $T_g$. Notably, an excessively high or low curing agent content may deteriorate shape memory performance. During the setting of the temporary shape, the reversible chain segments among the covalent bonds (i.e., crosslinked points) move at temperatures higher than $T_g$ and adapt to the external load via conformational rearrangements. Meanwhile, they become frozen when the temperature is below $T_g$. Strain energy is released when the SMEPs are unloaded and heated above their $T_g$ again, during which the original shape is restored. The DDM curing agent content directly influences cross-linking density, eventually leading to the varying performance of the SMEPs. These results will be highly significant in preparing for suitable and reliable shape memory polymers or composite materials when using epoxy resin E-51 and the curing agent DDM, and are in favor of extending further applications of these kind of smart polymers.

## ACKNOWLEDGEMENTS

This work was supported by the National Science Foundation of China [grant No. 51874329], National Science and Technology Major Project of China [2016ZX05020-004-009 and 2017ZX05009], National Natural Science Innovation Population of China [Grant No. 51821092], Major Program of the National Natural Science Foundation of China [Grant No. 51991361] and National Key Research and Development Project [2019YFB1504201].

## NOMENCLATURE

DDM : 4,4′-diaminodiphenyl methane
DGEBA : diglycidyl ether bisphenol A
DMA : dynamic mechanical analysis
DSC : differential scanning calorimetry
FTIR : fourier transform infrared spectroscopy
SMA : static mechanical analysis
SMEP : shape memory epoxy-based polymer
SMP : shape memory polymer
TGA : thermogravimetric analysis

## DATA AVAILABILITY

The raw/processed data required to reproduce these findings cannot be shared at this time as the data also forms part of an ongoing study.

## REFERENCES

1. A. Lendlein, *Shape-memory polymers*, Springer, Berlin/Heidelberg, Germany (2010).
2. J. Hu, *Shape memory polymers with novel functions: Electro-active, magnetically-active, light-adaptive and phase change materials*, Advances in Shape Memory Polymers; Woodhead Publishing:

Cambridge, UK (2013).
3. G. Tandon, J. Baur and A. McClung, *Shape memory polymers for aerospace applications: Novel synthesis, modeling, characterization and design*, DEStech Publications, Inc., Pennsylvania (2015).
4. J. Leng, X. Lan, Y. Liu and S. Du, *Prog. Mater. Sci.*, **56**(7), 1077 (2011).
5. L. Sun, W. M. Huang, Z. Ding, Y. Zhao, C. C. Wang, H. Purnawali and C. Tang, *Mater. Des.*, **33**, 577 (2012).
6. C. Liu, H. Qin and P. Mather, *J. Mater. Chem.*, **17**(16), 1543 (2007).
7. V. Beloshenko, Y. E. Beygelzimer, A. Borzenko and V. Varyukhin, *Compos. Part A*, **33**(7), 1001 (2002).
8. W. Du, Y. Jin, S. Lai, L. Shi, Y. Shen and H. Yang, *Compos. Part A*, **128**, 105686 (2020).
9. A. Nissenbaum, I. Greenfeld and H. D. Wagner, *Polymer*, **190**, 122226 (2020).
10. D. Yang, W. Huang, J. H. Yu, J. S. Jiang, L. Y. Zhang and M. R. Xie, *Polymer*, **51**(22), 5100 (2010).
11. G. Li, *Self-healing composites: shape memory polymer based structures*, John Wiley & Sons, West Sussex (2014).
12. L. Ma, J. Zhao, X. Wang, M. Chen, Y. Liang, Z. Wang, Z. Yu and R. C. Hedden, *Polymer*, **56**, 490 (2015).
13. I. S. Kolesov, K. Kratz, A. Lendlein and H.-J. Radusch, *Polymer*, **50**(23), 5490 (2009).
14. T. Ikematsu, Y. Kishimoto and M. Karaushi, Japan Patent, 02,022,355 (1990).
15. H. M. Jeong, B. K. Ahn and B. K. Kim, *Eur. Polym. J.*, **37**(11), 2245 (2001).
16. H. M. Jeong, J. H. Song, S. Y. Lee and B. K. Kim, *J. Mater. Sci.*, **36**(22), 5457 (2001).
17. L. T. J. Korley, B. D. Pate, E. L. Thomas and P. T. Hammond, *Polymer*, **47**(9), 3073 (2006).
18. Y. Zhu, J. L. Hu, K. F. Choi, Q. H. Meng, S. J. Chen and K. W Yeung, *Polym. Adv. Technol.*, **19**(4), 328 (2008).
19. H. Zhang, H. T. Wang, W. Zhong and Q. G. Du, *Polymer*, **50**(6), 1596 (2009).
20. D. Ratna and J. Karger-Kocsis, *J. Mater. Sci.*, **43**(1), 254 (2008).
21. J. D. Merline, C. P. R. Nair and K. N. Ninan, *J. Macromol. Sci., Part A: Pure Appl. Chem.*, **45**(4), 312 (2008).
22. K. S. Kumar, R. Biju and C. R. Nair, *React. Funct. Polym.*, **73**(2), 421 (2013).
23. Y. Liu, H. Du, L. Liu and J. Leng, *Smart Mater. Struct.*, **23**(2), 023001 (2014).
24. Y. Dong, M. Gong, D. Huang, J. Gao and Q. Zhou, *Prog. Org. Coat.*, **136**, 105232 (2019).
25. D. Margoy, I. Gouzman, E. Grossman, A. Bolker, N. Eliaz and R. Verker, *Acta Astronaut.*, **178**, 908 (2021).
26. S. Sun, G. Sun and J. Wu, *Smart Mater. Struct.*, **11**(6), 970 (2002).
27. A. Shimamoto, H. Zhao and T. Azakami, *Smart Mater. Struct.*, **16**(3), N13 (2007).
28. E. Kirkby, V. Michaud, J.-A. Månson, N. R. Sottos and S. R. White, *Polymer*, **50**(23), 5533 (2009).
29. A. Saeedi and M. M. Shokrieh, *J. Intell. Mater. Syst. Struct.*, **30**(10), 1585 (2019).
30. Z. Q. Wang, L. D. Xu, X. Y. Sun, M. F. Shi and J. B. Liu, *Compos. Struct.*, **178**, 311 (2017).
31. E. D'Elia, H. S. Ahmed, E. Feilden and E. Saiz, *Appl. Mater. Today*, **15**, 185 (2019).
32. M. H. M. Yazik, M. T. H. Sultan, N. Mazlan, A. R. A. Talib, J. Naveen, A. U. M. Shah and S. N. A. Safri, *J. Mater. Res. Technol.*, **9**(3), 6085 (2020).
33. Y. Yao, Y. Luo, Y. Xu, B. Wang, J. Li, H. Deng and H. Lu, *Compos. Part B*, **152**, 1 (2018).
34. Q. Fabrizio, S. Loredana and S. E. Anna, *Mater. Lett.*, **69**, 20 (2012).
35. T. Liu, L. Liu, M. Yu, Q. Li, C. Zeng, X. Lan, Y. Liu and J. Leng, *Compos. Struct.*, **206**, 164 (2018).
36. Y. Y. Liu, C. M. Han, H. F. Tan and X. W. Du, *Mater. Sci. Eng. A*, **527**(10-11), 2510 (2010).
37. W. B. Song, L. Y. Wang and Z. D. Wang, *Mater. Sci. Eng. A*, **529**, 29 (2011).
38. T. Xie and I. A. Rousseau, *Polymer*, **50**(8), 1852 (2009).
39. R. Hagen, L. Salmén and B. Stenberg, *J. Polym. Sci., Part B: Polym. Phys.*, **34**(12), 1997 (1996).
40. B. Saville and A. A. Watson, *Rubber Chem. Technol.*, **40**(1), 100 (1967).
41. J. Karger-Kocsis and S. Kéki, *Polymer*, **10**(1), 34 (2018).
42. B. A. Nelson, W. P. King and K. Gall, *Appl. Phys. Lett.*, **86**(10), 103108 (2005).